

# AN ALGORITHM TO COMPUTE SOME HEEGAARD FLOER HOMOLOGIES

SUCHARIT SARKAR AND JIAJUN WANG

ABSTRACT. In this paper, we give an algorithm to compute the hat version of the Heegaard Floer homology of a closed oriented three-manifold. This method also allows us to compute the filtrations coming from a null-homologous link in a three-manifold.

## 1. INTRODUCTION

Heegaard Floer homology is a collection of invariants for closed oriented three-manifolds, introduced by Peter Ozsváth and Zoltán Szabó [7, 8]. There are four versions, denoted by  $\widehat{HF}$ ,  $HF^\infty$ ,  $HF^+$  and  $HF^-$ , which are graded abelian groups satisfying certain long exact sequences. Specifically,  $HF^-$  is a homology group with coefficients in  $\mathbb{Z}[U]$  and  $\widehat{HF}$  is obtained by setting  $U = 0$ .

A cobordism between two three-manifolds induces homomorphisms on the Heegaard Floer homology groups of the two three-manifolds. In fact, the homomorphisms on  $HF^-$  and  $HF^+$  can be used to construct an invariant of smooth four-manifolds with  $b_2^+ > 1$  ([10]), called the Ozsváth-Szabó invariant. Conjecturally, the Ozsváth-Szabó four-manifold invariant is equivalent to the gauge-theoretic Seiberg-Witten invariant.

We shall mostly be concerned with the hat version Heegaard Floer homology. A null-homologous knot  $K \subset Y$  with a Seifert surface  $S$  induces a filtration of the chain complex  $\widehat{CF}(Y)$ , and each filtration level is a knot invariant. The homology groups  $\widehat{HFK}(Y, K)$  of successive quotients of filtration levels is called knot Floer homology. Knot Floer homology was discovered independently by Peter Ozsváth and Zoltán Szabó [11] and by Jacob Rasmussen [17]. Knot Floer homology is bi-graded and the two gradings are called the homology and Alexander gradings. For a knot  $K$  in the three-sphere  $S^3$ , the Euler characteristic of  $\widehat{HFK}(S^3, K)$  along the homology grading gives the Alexander polynomial  $\Delta_K(t)$  of  $K$ . For an  $l$ -component link, there is a  $(l + 1)$ -graded version of the homology group ([14]), the link Floer homology.

Heegaard Floer homology turns out to be a fruitful and powerful theory in the study of three- and four-dimensional topology. It gives simpler proof of the Donaldson diagonalizable theorem and Thom conjecture for  $\mathbb{C}P^2$  ([9]). Moreover, knot Floer homology detects the genus ([12]) and fibredness ([1, 6, 2]) of knots and links in the three-sphere. And link Floer homology detects the Thurston norm of links in the three-sphere ([15]). An invariant  $\tau$  coming from the knot filtration whose absolute value gives a lower-bound of the slice genus for knots in the three-sphere ([13]).

All these invariants are constructed after taking a Heegaard diagram of the three-manifold  $Y$  with some basepoint  $w$  (and another basepoint  $z$  in case we are taking a knot in  $Y$ ). The differentials count the number of points in certain moduli spaces, which are hard to describe in general. It is a challenging problem to find a combinatorial description of these theories.

In this paper, we give an algorithm to compute  $\widehat{HF}(Y)$  for a three-manifold  $Y$ , and also  $\widehat{HFK}(Y, K)$  for a knot  $K$  in any three-manifold. All our computations will be done with coefficients in  $\mathbb{F}_2 = \mathbb{Z}/2\mathbb{Z}$ . We shall be trying to find a nice Heegaard diagram satisfying certain property (Definition 3.1), and with such Heegaard diagrams it will be easy to compute  $\widehat{HF}$  and  $\widehat{HFK}$ . Our main results are summarized in the following theorems.

---

1991 *Mathematics Subject Classification*. Primary 57R58.

*Key words and phrases*. Heegaard Floer homology; knot Floer homology; algorithm.

**Theorem 1.1.** *For a nice Heegaard diagram of a closed oriented three-manifold  $Y$ ,  $\widehat{HF}(Y)$  can be computed combinatorially. Similarly, for a knot  $K \subset Y$ ,  $\widehat{HFK}(Y, K)$  can be computed combinatorially in a nice Heegaard diagram.*

**Theorem 1.2.** *Every closed oriented three-manifold  $Y$  admits a nice Heegaard diagram. And for a null-homologous knot  $K$  in a closed oriented three-manifold  $Y$ , the pair  $(Y, K)$  admits a compatible nice Heegaard diagram. In fact, every pointed Heegaard diagram can be made nice via isotopies and handleslides.*

It will be interesting to compare our result with the recent work of Ciprian Manolescu, Peter Ozsváth and the first author in [5], where they gave a combinatorial description of knot Floer homology of knots in  $S^3$ , in all versions.

We remark that we do not know whether this method can be generalized to compute some of the other versions, notably  $HF^-(Y)$  and  $HF^+(Y)$ . Also, the proof of the invariance of the combinatorial description still relies on the Heegaard Floer theory using holomorphic disks.

The paper is organized as follows. In Section 2, we give an overview of certain concepts in Heegaard Floer theory. In Section 3, we give a combinatorial characterization of index one pseudo-holomorphic disks missing the basepoint  $w$  in a special class of Heegaard diagrams. In Section 4, we give an algorithm to get such Heegaard diagrams. In Section 5, we give examples to demonstrate our algorithm for three-manifolds and knots in the three-sphere.

#### ACKNOWLEDGEMENT

The first author wishes to thank Zoltán Szabó for introducing him to the subject of Heegaard Floer homology and having many helpful discussions at various points. He also wishes to thank Matthew Hedden and Robert Lipshitz for their comments.

This work was done when the second author was an exchange graduate student in Columbia University. He is grateful to the Columbia math department for its hospitality. He also would like to thank Rob Kirby and Peter Ozsváth for their continuous guidance, support and encouragement.

We thank Ciprian Manolescu, Peter Ozsváth and Dylan Thurston for making comments and having helpful discussions during the development of this work.

We also thank the referees for their comments and suggestions.

## 2. PRELIMINARIES

In this section, we review the definition of the hat version Heegaard Floer homology. See [7, 8, 3] for more details.

Given a closed oriented three-manifold  $Y$ , we fix a self-indexing Morse function  $f$  with  $k$  index zero critical points and  $k$  index three critical points on  $Y$ . We fix a gradient like flow on  $Y$  corresponding to  $f$ . In case we have a link  $L$  in  $Y$ , we ensure that  $L$  is made out of flow lines from index zero critical points to index three critical points, and  $L$  contains all index one and index three critical points and no index one and two critical points.

If the number of index one critical points or the number of index two critical points of  $f$  is  $(g + k - 1)$ , then  $\Sigma = f^{-1}(3/2)$  will be a genus  $g$  surface. We then get a collection of  $(g + k - 1)$   $\alpha$  circles on  $\Sigma$  which flow down to the index one critical points, and another collection of  $(g + k - 1)$   $\beta$  circles on  $\Sigma$  which flow up to the index two critical points.

We fix  $k$  basepoints  $w_1, w_2, \dots, w_k$  in the complement of the  $\alpha$  circles and the  $\beta$  circles in  $\Sigma$ , such that their trajectories under the gradient like flow hit all the index zero and all the index three critical points. In case we had a link in  $Y$ , we orient the link and  $\Sigma$ , and we define the basepoints  $w_i$  as the positive intersection points between the link and  $\Sigma$ . We write the other  $k$  intersections as  $z_i, 1 \leq i \leq k$ .

Thus the three-manifold  $Y$  is represented by  $(\Sigma_g, \boldsymbol{\alpha}, \boldsymbol{\beta}, \mathbf{w})$ , where  $\mathbf{w} = (w_1, \dots, w_k)$  and  $\boldsymbol{\alpha} = (\alpha_1, \dots, \alpha_{g+k-1})$  (resp.  $\boldsymbol{\beta} = (\beta_1, \dots, \beta_{g+k-1})$ ) contains  $(g+k-1)$  disjoint circles whose complement  $\Sigma \setminus \boldsymbol{\alpha}$  (resp.  $\Sigma \setminus \boldsymbol{\beta}$ ) has  $k$  components each of which contains some  $w_i$ . For a link  $K \subset Y$  with  $k$  components, we have  $k$  extra basepoints  $z_1, \dots, z_k$  such that each component of  $\Sigma \setminus \boldsymbol{\alpha}$  (resp.  $\Sigma \setminus \boldsymbol{\beta}$ ) contains some  $z_i$ . Such a diagram is called a *pointed Heegaard diagram*.

In the hat version Heegaard Floer homology, the generators of the chain complex are given by formal sums of  $(g+k-1)$  distinct points in  $\Sigma$ ,  $\mathbf{x} = x_1 + \dots + x_{g+k-1}$ , such that each  $\alpha$  (resp.  $\beta$ ) circle contains some  $x_i$ . We define a connected component of  $\Sigma \setminus (\boldsymbol{\alpha} \cup \boldsymbol{\beta})$  to be a *region*. Given two generators  $\mathbf{x}$  and  $\mathbf{y}$ , we define  $\pi_2(\mathbf{x}, \mathbf{y})$  to be the collection of all 2-chains  $\phi$  generated freely by the regions, such that  $\partial(\partial(\phi)|_\alpha) = \mathbf{y} - \mathbf{x}$ . We often call such 2-chains to be *domains*. Given a point  $p \in \Sigma \setminus (\boldsymbol{\alpha} \cup \boldsymbol{\beta})$ , we define  $n_p(\phi)$  as the coefficient of  $\phi$  at the region containing  $p$ . We call a domain  $\phi$  to be *positive* if  $n_p(\phi) \geq 0 \forall p$ . We define  $\pi_2^0(\mathbf{x}, \mathbf{y}) = \{\phi \in \pi_2(\mathbf{x}, \mathbf{y}) | n_{w_i}(\phi) = 0 \forall i\}$ .

If the three-manifold  $Y$  has  $b_1(Y) > 0$ , we require the Heegaard diagram to be admissible. A diagram is *admissible*, if, for every generator  $\mathbf{x}$ , any positive domain  $P \in \pi_2^0(\mathbf{x}, \mathbf{x})$  is in fact a trivial domain.

For a generator  $\mathbf{x} = \sum x_i$  and a two-chain  $\phi$ , we define  $\mu_{x_i}(\phi)$  to be average of the coefficients of  $\phi$  in the four regions around  $x_i$ , and we define  $\mu_{\mathbf{x}}(\phi) = \sum \mu_{x_i}(\phi)$ .

If we fix a metric on  $\Sigma$  which makes all the  $\alpha$  circles and all the  $\beta$  circles geodesics, intersecting each other at right angles, then  $e(\phi)$  is defined to be  $\frac{1}{2\pi}$  of the integral of the curvature on  $\phi$ . Thus  $e$  is clearly additive, if  $D$  is a  $2n$ -gon region, then  $e(D) = 1 - \frac{n}{2}$ .

Given  $\phi \in \pi_2(\mathbf{x}, \mathbf{y})$ , the Maslov index of  $\phi$  can be computed by Lipshitz's formula ([3]) as  $\mu(\phi) = e(\phi) + \mu_{\mathbf{x}}(\phi) + \mu_{\mathbf{y}}(\phi)$ . The boundary map in the hat version is given by

$$\partial \mathbf{x} = \sum_{\mathbf{y}} \sum_{\phi \in \pi_2^0(\mathbf{x}, \mathbf{y}), \mu(\phi)=1} c(\phi) \mathbf{y},$$

where  $c(\phi)$  is the *count function*, which counts the number of pseudo-holomorphic disks in certain symmetric product of the Heegaard Surface (See [7] for details).

For a null-homologous link in  $Y$ ,  $\sum n_{z_i}(\phi)$  gives a filtration of  $\widehat{CF}(Y)$ . The homology of this chain complex depends only on  $Y$  (or the link in  $Y$ ) and  $k$ . Increasing  $k$  by 1 corresponds to tensoring the homology by  $\mathbb{F}_2^2$ . For three-manifolds, we generally choose  $k = 1$ , and for links with  $l$  components, we choose  $k = l$ .

In the following, we shall be using the reformulation of Lipshitz [3]. The count function  $c(\phi)$  is the only non-combinatorial part in the whole theory. We consider all surfaces  $S$  with boundary, with  $2(g+k-1)$  marked points  $(X_1, \dots, X_{g+k-1}, Y_1, \dots, Y_{g+k-1})$  on  $\partial S$ , such that the  $2(g+k-1)$  arcs on  $\partial S$  in the complement of the marked points are subdivided into two groups  $A$  and  $B$  containing  $(g+k-1)$  arcs each. We look at maps  $u : S \rightarrow \Sigma \times D^2$ , such that under the first projection  $p_1$ , the image is  $\phi$ , with  $X$  (resp.  $Y$ ) points mapping injectively to  $x$  (resp.  $y$ ),  $A$  (resp.  $B$ ) arcs mapping to  $\alpha$  (resp.  $\beta$ ) arcs, and under the second projection  $p_2$ , the image is  $(g+k-1)D^2$ , with  $X$  (resp.  $Y$ ) points mapping to  $-i$  (resp.  $i$ ) in the unit disk, and  $A$  (resp.  $B$ ) arcs mapping to the arc in  $\partial(D^2)$  joining  $-i$  to  $i$  in half-plane  $Re(s) > 0$  (resp.  $Re(s) < 0$ ). We fix a complex structures on  $\Sigma$  and  $D^2$  and take the product complex structure on  $\Sigma \times D^2$ , and if that complex structure achieves some sort of transversality for  $\phi$ , then the count  $c(\phi)$  is the number of holomorphic embedding of this type, up to the one-parameter family of diffeomorphisms of  $D^2 \setminus \{i, -i\}$ .

If a domain  $\phi$  which actually supports some holomorphic curve  $f$  then  $n_p(\phi)$  is simply the intersection of  $f(S)$  and  $\{p\} \times D^2$ , and both of them being holomorphic objects in product complex structure, they have positive intersection and hence  $n_p(\phi) \geq 0$ . So if  $\phi$  supports a holomorphic curve,  $\phi$  is a positive domain. Also in that case, the number of branch points of  $p_2 \circ u$  is given by  $\mu_{\mathbf{x}} + \mu_{\mathbf{y}} - e(\phi)$  ([3, 17]). Furthermore, in such a situation Maslov index has other reformulations as  $\mu(\phi) = 2e(\phi) + g + k - 1 - \chi(S) = e(\phi) + b + \frac{1}{2}(g + k - 1 - t)$ , where  $b$  denotes the number of

branch points of  $p_1 \circ u$ , and  $t$  denotes number of trivial disks, i.e. the components of  $S$  which map to a point by  $p_1 \circ u$  (which correspond to coordinates  $x_i$  of  $\mathbf{x}$  with  $\mu_{x_i} = 0$ ). The condition that  $\mu(\phi) = 1$  is simply the condition that the expected dimension of the unparametrized moduli space of embeddings is 0.

### 3. HOLOMORPHIC DISKS IN NICE HEEGAARD DIAGRAMS

In this section, we study index one pseudo-holomorphic disks in nice Heegaard diagrams.

**Definition 3.1.** Let  $\mathcal{H} = (\Sigma, \boldsymbol{\alpha}, \boldsymbol{\beta}, \mathbf{w})$  be a pointed Heegaard diagram for a three-manifold  $Y$ .  $\mathcal{H}$  is called **nice** if all regions that do not contain any points  $w_i$  in  $\mathbf{w}$  are either bigons or squares.

Let us assume that we have a nice admissible Heegaard diagram for a closed oriented three-manifold  $Y$ . We choose a product complex structure on  $\Sigma \times D^2$ .

We call a domain  $\phi \in \pi_2^0(\mathbf{x}, \mathbf{y})$  to be an empty embedded  $2n$ -gon, if the domain has coefficients 0 and 1 everywhere, and is topologically an embedded disk, with  $2n$  vertices on its boundary, such that at each vertex  $v$ ,  $\mu_v(\phi) = \frac{1}{4}$ , and it does not contain any  $x$ -coordinate in its interior.

**Theorem 3.2.** If  $\phi \in \pi_2^0(\mathbf{x}, \mathbf{y})$  with  $\mu(\phi) = 1$  has a holomorphic representative, then  $\phi$  is an empty embedded bigon or an empty embedded square.

*Proof.* Let  $\phi = \sum a_i D_i$ , where  $D_i$ 's are regions not containing the basepoints. Hence each  $D_i$  is a bigon or a square, and so  $e(D_i) \geq 0$ . Also since  $\phi$  has a holomorphic representative  $a_i \geq 0 \forall i$ .

By Lipshitz' formula  $\mu(\phi) = e(\phi) + \mu_{\mathbf{x}}(\phi) + \mu_{\mathbf{y}}(\phi)$ , and  $e(\phi) = \sum a_i e(D_i) \geq 0$ . Thus  $0 \leq \mu_{\mathbf{x}} + \mu_{\mathbf{y}} \leq 1$ .

Now let  $\mathbf{x} = x_1 + x_2 + \dots + x_g$  and  $\mathbf{y} = y_1 + y_2 + \dots + y_g$ , with  $x_i, y_i \in \alpha_i$ . We say  $\phi$  hits some  $\alpha$  circle if  $\partial\phi$  is non-zero on some part of that  $\alpha$  circle. Since  $\phi \neq n\Sigma$ , it has to hit at least one  $\alpha$  circle, say  $\alpha_1$  and hence (as  $\partial(\partial\phi|_{\alpha}) = \mathbf{y} - \mathbf{x}$ ),  $\mu_{x_1}, \mu_{y_1} \geq \frac{1}{4}$ . Also if  $\phi$  does not hit  $\alpha_i$ , then  $x_i = y_i$ , and if possible say  $\mu_{x_i} \neq 0$ , then  $\mu_{x_i} = \mu_{y_i} \geq \frac{1}{2}$ , and hence  $\mu_{\mathbf{x}} + \mu_{\mathbf{y}}$  becomes too large. Thus if  $\phi$  does not hit  $\alpha_i$ ,  $x_i = y_i$  lies outside the domain  $\phi$ .

We now note that  $e(\phi)$  can only take half-integral values, and thus only the following cases might occur.

- $\phi$  hits  $\alpha_1$  and  $\alpha_2$ ,  $\phi$  consists of squares,  $\mu_{x_1} = \mu_{x_2} = \mu_{y_1} = \mu_{y_2} = \frac{1}{4}$ , there are  $(g + k - 3)$  trivial disks.
- $\phi$  hits  $\alpha_1$ ,  $D(\phi)$  consists of squares,  $\mu_{x_1} + \mu_{y_1} = 1$ , there are  $(g + k - 2)$  trivial disks.
- $\phi$  hits  $\alpha_1$ ,  $D(\phi)$  consists of squares and exactly one bigon,  $\mu_{x_1} = \mu_{y_1} = \frac{1}{4}$ , there are  $(g + k - 2)$  trivial disks

The first case corresponds to a map from  $S$  to  $\Sigma$  with  $\chi(S) = (g + k - 2)$ , and  $S$  has  $(g + k - 3)$  trivial disk components. If the rest of  $S$  is  $F$ , then  $F$  is a double branched cover over  $D^2$  with  $\chi(F) = 1$  and 1 branch point (for holomorphic maps, the number of branch points is given by  $\mu_{\mathbf{x}} + \mu_{\mathbf{y}} - e(\phi)$ ), i.e.  $F$  is a disk with 4 marked points on its boundary. Call the marked points corners, and call  $F$  a square.

In the other cases,  $S$  has  $(g + k - 2)$  trivial disk components, so if  $F$  denote the rest of  $S$ , then  $F$  is just a single cover over the disk. Thus the number of branch points has to be 0. But in the second case the number of branch points is 1, so the second case cannot occur. In the third case,  $F$  is a disk with 2 marked points on its boundary. Again call the marked points corners, and call  $F$  a bigon.

Thus in both these cases,  $\phi$  is the image of  $F$  and all the trivial disks map to  $x$ -coordinates (which are also  $y$ -coordinates) which do not lie in  $\phi$ . Note that in both cases, the map from  $F$  to  $\phi$  has no branch point, so it is a local diffeomorphism, even at the boundary of  $F$ . Furthermore using the condition that  $\mu_{x_i}$  (or  $\mu_{y_i}$ ) =  $\frac{1}{4}$  whenever it is non-zero, we conclude that there is exactly one preimage for the image of each corner of  $F$ .

All we need to show is that the map from  $F$  to  $\Sigma$  is an embedding, or in other words the local diffeomorphism from  $F$  to  $\phi$  is actually a diffeomorphism.

We shall be concentrating on the case of  $F$  being a square in more details, but the other case is similar.

**Case 1.** In this case we have an immersion  $f : F \rightarrow \Sigma$ , where  $F$  is a square (with boundary). Look at the preimage of all the  $\alpha$  and  $\beta$  circles in  $F$ . Using the fact  $f$  is a local diffeomorphism, we see that each of the preimages of  $\alpha$  and  $\beta$  arcs are also 1-manifolds, and by an abuse of notation, we shall also be calling them  $\alpha$  or  $\beta$  arcs. Using the embedding condition near the 4 corners, we see that at each corner only one  $\alpha$  arc and only one  $\beta$  arc can come in. The different  $\alpha$  arcs cannot intersect and the different  $\beta$  arcs cannot intersect, and all intersections between  $\alpha$  and  $\beta$  arcs are transverse.

Note that since the preimage of each square region is a square, so  $F$  (with all the  $\alpha$  and  $\beta$  arcs) is also tiled by squares. Thus the  $\alpha$  arcs in  $F$  cannot form a closed loop, for in that case  $F \setminus \{\text{inside of loop}\}$  has  $e$  negative and hence cannot be tiled by squares. Similarly the  $\beta$  arcs cannot form a loop. Also no  $\alpha$  arc can enter and leave  $F$  through the same  $\beta$  arc on the boundary, for again the outside will have negative  $e$ . Thus the  $\alpha$  arcs slice up  $F$  into vertical rectangles, and in each rectangle, no  $\beta$  arc can enter and leave through the same  $\alpha$  arc. This shows that the  $\alpha$  arcs and  $\beta$  arcs make the standard co-ordinate chart on  $F$ .

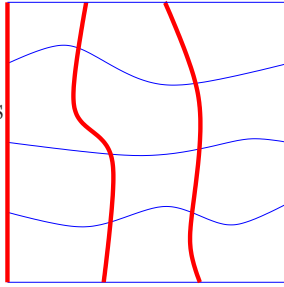


FIGURE 1. **Preimage of  $\alpha$  and  $\beta$  arcs for a square.** We make the convention in all figures in the paper that the thick solid arcs denote  $\alpha$  arcs and the thin solid arcs denote  $\beta$  arcs.

We call the intersection points between  $\alpha$  and  $\beta$  arcs in  $F$  vertices (and we are still calling the four original vertices on the boundary of the square  $F$  corners). Note that to show  $f$  is an embedding, it is enough to show that no two different vertices map to the same point. Assume  $p, q \in F$  are distinct vertices with  $f(p) = f(q)$ . There could be two subcases.

- Both  $p$  and  $q$  are in  $\overset{\circ}{F}$ .
- At least one of  $p$  and  $q$  is in  $\partial F$ .

We shall be reducing the first subcase to the second. So assume both are in the interior of  $F$ . Choose a direction on the  $\alpha$  arc passing through  $f(p) = f(q)$  in  $\Sigma$ , and keep looking at successive points of intersection with  $\beta$  arcs, and locate their inverse images in  $F$ . For each point, we shall get at least a pair of inverse images, one on the  $\alpha$  arc through  $p$ , and one on the  $\alpha$  arc through  $q$ , until one of the points falls on  $\partial F$ , and thus the reduction the second subcase.

In this subcase, without loss of generality, we assume that  $p$  lies on a  $\beta$  arc in  $\partial F$ . Then choose a direction on the  $\beta$  arc in  $\Sigma$  through  $f(p) = f(q)$  and proceed as above, until one of the preimages hits an  $\alpha$  arc on  $\partial F$ . If that preimage is on the  $\beta$  arc through  $q$ , then reverse the direction and proceed again, and this time we can ensure that the preimage which hits  $\alpha$  arc on  $\partial F$  first is the one that was on the  $\beta$  arc through  $p$ . Thus we get 2 distinct vertices in  $F$  mapping to the same point in  $\Sigma$ , one of them being a corner. This is a contradiction to the embedding assumption near the corners.

**Case 2.** In this case we have  $f : F \rightarrow \Sigma$  an immersion with  $F$  being a bigon. Again look at the preimage of  $\alpha$  and  $\beta$  circles. All intersections will be transverse (call them vertices), and at each of the 2 corners there can be only one  $\alpha$  arc and only one  $\beta$  arc. Again there cannot be any closed loops. We get an induced tiling on  $F$  with squares and 1 bigon.

But this time the  $\alpha$  arcs can (in fact they have to) enter and leave  $F$  through the same  $\beta$  arc, but they do have to do it in a completely nested fashion (i.e. there is only one innermost bigon). Thus  $F$  decomposes into at most two pieces, the innermost bigon and the rest. In case there were no  $\alpha$  arcs in  $F$ , the rest might be empty, but otherwise it is a square. From the earlier case,  $\beta$  arcs must cut up the square piece in a standard way, and from the previous argument, the  $\beta$  arcs must enter and leave the bigon in a nested fashion.

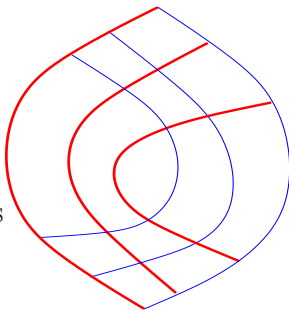


FIGURE 2. Preimage of  $\alpha$  and  $\beta$  arcs for a bigon.

Again to show  $f$  is an embedding, enough to show that it is an embedding restricted to vertices. Take 2 distinct vertices  $p, q$  mapping to the same point, and follow them along  $\alpha$  arcs in some direction, until one of them hits a  $\beta$  arc on  $\partial F$ . Then follow them along  $\beta$  arcs, and  $\exists$  some direction such that one of them will actually hit a corner, giving the required contradiction.

So in either case,  $f$  is an embedding.  $\square$

**Theorem 3.3.** *If  $\phi \in \pi_2^0(\mathbf{x}, \mathbf{y})$  is an empty embedded bigon or an empty embedded square, then  $\mu(\phi) = 1$  and under a generic perturbation of the  $\alpha$  and the  $\beta$  circles, the product complex structure achieves transversality for  $\phi$ , and  $c(\phi) = 1$ .*

*Proof.* Let  $\phi$  be an empty  $2n$ -gon. Each of the corners of  $\phi$  must be an  $x$ -coordinate or a  $y$ -coordinate, and at every other  $x$  (resp.  $y$ ) coordinate  $\mu_{x_i}$  (resp.  $\mu_{y_i}$ ) is zero. So  $\mu_{\mathbf{x}}(\phi) + \mu_{\mathbf{y}}(\phi) = 2n \cdot \frac{1}{4} = \frac{n}{2}$ .

Also  $\phi$  is topologically a disk, so it has Euler characteristic 1. But since it has  $2n$  corners each with an angle of  $\frac{\pi}{4}$ , the Euler measure  $e(\phi) = 1 - \frac{2n}{4} = 1 - \frac{n}{2}$ . Thus  $\mu(\phi) = 1$ .

Also using [3, Lemma 3.7], we see that  $\phi$  satisfies boundary injective condition, and hence under a generic perturbation of the  $\alpha$  and the  $\beta$  circles, the product complex structure achieves transversality for  $\phi$ .

When  $\phi$  is a square, we can choose  $F$  to be square which maps to  $\phi$  diffeomorphically. A complex structure on  $\Sigma$  induces a complex structure on  $F$ , and given a complex structure on  $F$  (which is a disk with 4 marked points on its boundary), there is a unique holomorphic branched cover  $F \rightarrow D^2$  satisfying boundary conditions and up to reparametrization. Thus  $\phi$  has a holomorphic representative, and from the proof of the previous theorem we see that this fixes  $F$ , and thus this is the unique holomorphic representative.

When  $\phi$  is a bigon, we can choose  $F$  to be a bigon which maps to  $\phi$  diffeomorphically. A complex structure on  $\Sigma$  induces a complex structure on  $F$ , and then there is a unique holomorphic map from  $F$  to the standard  $D^2$  after reparametrization. Thus again  $\phi$  has a holomorphic representative, and hence similarly it must be the unique one.  $\square$

**Proof of Theorem 1.1.** Theorem 3.2 and 3.3 make the count function  $c(\phi)$  in a nice Heegaard diagram combinatorial. For  $\phi \in \pi_2^0(\mathbf{x}, \mathbf{y})$ ,  $c(\phi) = 1$  if  $\phi$  is an empty embedded bigon or an empty embedded rectangle, and is 0 otherwise.  $\square$

4. ALGORITHM TO GET NICE HEEGAARD DIAGRAMS

In this section, we prove Theorem 1.2. We will demonstrate an algorithm which, starting with an admissible pointed Heegaard diagram, gives an admissible nice Heegaard diagram by doing isotopies and handleslides on the  $\beta$  curves.

In most part of this section, we consider a Heegaard diagram with a single basepoint, and we consider Heegaard diagrams with more basepoints in the last subsection.

For a Heegaard diagram, a disk region is a  $2n$ -gon if its boundary contains  $n$   $\alpha$  edges. We call bigon and square regions *good* and all other regions *bad*.

Let  $\mathcal{H} = (\Sigma, \alpha, \beta, w)$  be a pointed Heegaard diagram with a single basepoint  $w$ .

**4.1. Killing non-disk regions.** If  $\alpha_i$  does not intersect any  $\beta$  circle, we can find an arc  $c$  to connect  $\alpha_i$  to some  $\beta_j$  avoiding the intersections of  $\alpha$  and  $\beta$  circles, as indicated in Figure 3(a). And we could select  $c$  so that  $c$  intersects  $\beta$  just at the endpoint. Doing a finger move of  $\beta_j$  along  $c$  as in Figure 3(b) will make  $\alpha_i$  intersect some  $\beta$  circle.

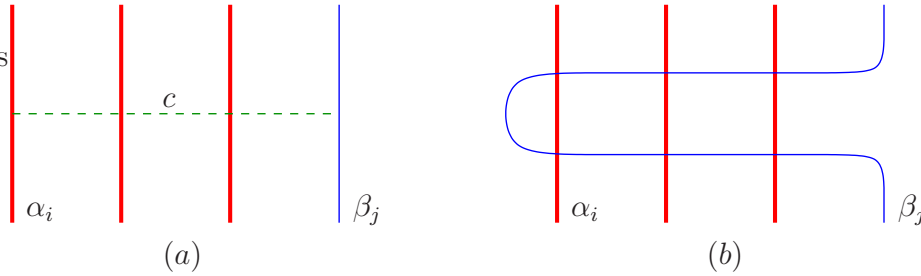


FIGURE 3. Making each  $\alpha$  circle intersect some  $\beta$  circle.

Similarly, if  $\beta_i$  does not intersect any  $\alpha$  circle, we find an arc  $c$  connecting  $\beta_i$  to some  $\alpha_j$  so that  $c \cap \alpha$  contains a single point as in Figure 4(a). And we do the operation in Figure 4(b).

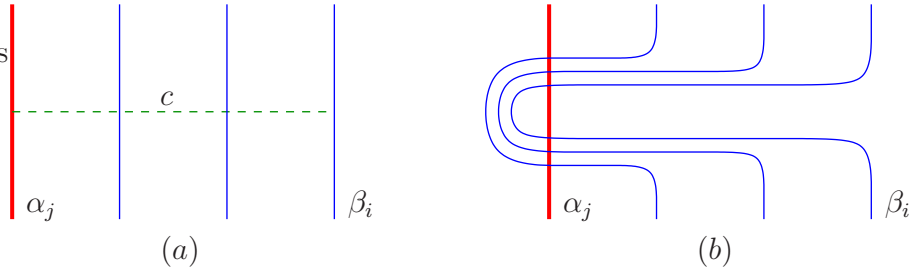


FIGURE 4. Making each  $\beta$  circle intersect some  $\alpha$  circle.

Repeating the above process, we can make sure that every  $\alpha$  circle intersects some  $\beta$  circle and every  $\beta$  circle intersects some  $\alpha$  circle.

Note that the complement of the  $\alpha$  curves is a punctured sphere. So every region is a planar surface. A non-disk region  $D$  has more than one boundary component. Every boundary component must contain both  $\alpha$  and  $\beta$  arcs since every  $\alpha$  (resp.  $\beta$ ) circle intersects some  $\beta$  (resp.  $\alpha$ ) circle. Then we make a finger move on the  $\beta$  curve to reduce the number of boundary components of  $D$  without generating other non-disk regions. See Figure 5 for this finger move operation. Repeating this process as many times as necessary, we will kill all non-disk regions.

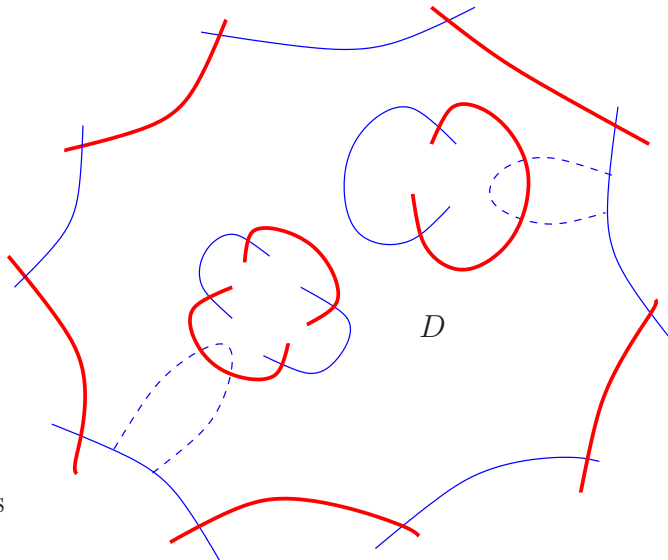


FIGURE 5. **Killing non-disk regions.** The dotted arcs indicates our finger moves. After our finger move, the region  $D$  becomes a disk region.

**4.2. Making all but one region bigons or squares.** In this subsection, we just consider Heegaard diagrams with only disk regions. Note that our algorithm will not generate non-disk regions.

Let  $D_0$  be the disk region containing the basepoint  $w$ . For any region  $D$ , pick an interior point  $w' \in D$  and define the *distance* of  $D$ , denoted by  $d(D)$ , to be the smallest number of intersection points of an arc (disjoint from  $\alpha$  curves) connecting  $w$  and  $w'$ , with the  $\beta$  curves. For a  $2n$ -gon disk region  $D$ , define the *badness* of  $D$  to be  $b(D) = \max\{n - 2, 0\}$ .

For a pointed Heegaard diagram  $\mathcal{H}$  with only disk regions, define the *distance*  $d(\mathcal{H})$  of  $\mathcal{H}$  to be the largest distance of bad regions. Define the *distance  $d$  complexity* of  $\mathcal{H}$  to be tuple

$$c_d(\mathcal{H}) = \left( \sum_{i=1}^m b(D_i), -b(D_1), -b(D_2), \dots, -b(D_m) \right),$$

where  $D_1, \dots, D_m$  are all the distance  $d$  bad regions, ordered so that  $b(D_1) \geq b(D_2) \geq \dots \geq b(D_m)$ . We call the first term the *total badness of distance  $d$*  of  $\mathcal{H}$ , and denote by  $b_d(\mathcal{H})$ . If there are no distance  $d$  bad regions, then  $c_d(\mathcal{H}) = (0)$ . We order the set of distance  $d$  complexities lexicographically.

**Lemma 4.1.** *For a distance  $d$  pointed Heegaard diagram  $\mathcal{H}$  with only disk regions, if  $c_d(\mathcal{H}) \neq (0)$ , we can modify  $\mathcal{H}$  by isotopies and handleslides to get a new Heegaard diagram  $\mathcal{H}'$  with only disk regions, satisfying  $d(\mathcal{H}') \leq d(\mathcal{H})$  and  $c_d(\mathcal{H}') < c_d(\mathcal{H})$ .*

*Proof.* We order the bad regions of distance  $d$  as in the definition of the distance  $d$  complexity. Now we look at  $D_m$ . It is a  $(2n)$ -gon with  $n \geq 3$ . Pick an adjacent region  $D_*$  with distance  $d - 1$  having a common  $\beta$  edge with  $D_m$ . Let  $b_*$  be (one of) their common  $\beta$  edge(s). We order the  $\alpha$  edges of  $D_m$  counterclockwise, and denote them by  $a_1, a_2, \dots, a_n$  starting at  $b_*$ .

We try to make a finger move on  $b_*$  into the  $D_m$  and out of  $D_m$  through  $a_2$ , as indicated in Figure 6 when  $D_m$  is an octogen. Our finger will separate  $D_m$  into two parts,  $D_{m,1}$  and  $D_{m,2}$ .

If we reach a square region of distance  $\geq d$ , we push up our finger outside the region via the opposite edge, as in Figure 7. Note that doing a finger move through regions of distance  $\geq d$  does not change the distance of any of the bad regions, since they all have distance  $\leq d$ .

We continue to push up our finger as far as possible, until we reach one of the following:

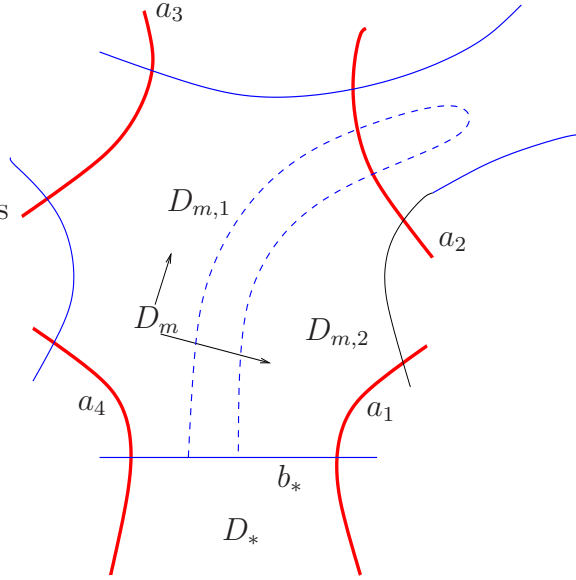


FIGURE 6. Starting our finger move.

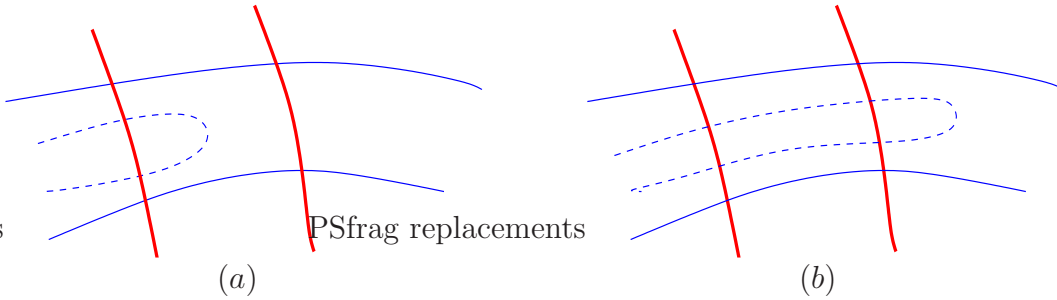


FIGURE 7. Moving across a square region.

- (1) a bigon region.
- (2) a region with distance  $\leq d - 1$ .
- (3) a bad region with distance  $d$  other than  $D$ , i.e.,  $D_i$  with  $i < m$ .
- (4)  $D_m$ .

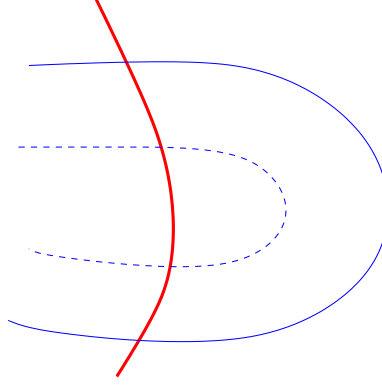
We will prove our lemma case by case.

**Case 1. A bigon is reached.**

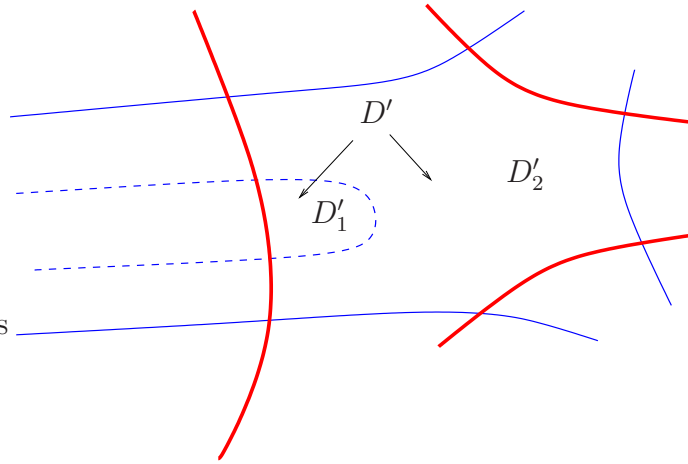
Before we reach the bigon region, all regions in between are square regions with distance  $\geq d$ . And after our finger moves inside a bigon region, our finger separates the bigon into a square and a new bigon. See Figure 8 for the bigon case.

Denote the new Heegaard diagram by  $\mathcal{H}'$ . We have  $b(D_{m,1}) = b(D_m) - 1$ . Since  $D_{m,2}$  is a square and is good, we get  $b_d(\mathcal{H}') = b_d(\mathcal{H}) - 1$ . Note that we will not increase the distance of any distance  $d$  bad region since we do not pass any region of distance  $\leq d - 1$ . So  $d(\mathcal{H}') \leq d(\mathcal{H})$  and  $c_d(\mathcal{H}') < c_d(\mathcal{H})$ .

**Case 2. A smaller distance region is reached.**

FIGURE 8. **Case 1. A bigon is reached.**

Let  $D'$  be the region with distance  $< d$  we reached by our finger. Suppose  $d(D') = d'$ . Let  $\mathcal{H}'$  be the new Heegaard diagram. See Figure 9. Note that  $D'$  might be a bigon, which could be covered in both Case 1 and Case 2.

FIGURE 9. **Case 2. A smaller distance region is reached.**

We have  $b(D_{m,1}) = b(D_m) - 1$  and  $D_{m,2}$  is good. Our finger separates  $D'$  into a bigon region  $D'_1$  and the other part  $D'_2$ . When  $D'$  is a square or a bad region,  $D'_2$  will be a bad region of distance  $d' < d$ . Certainly we have increased the distance  $d'$  complexity. But we have  $d(\mathcal{H}') \leq d(\mathcal{H})$  and  $c_d(\mathcal{H}') < c_d(\mathcal{H})$ .

**Case 3. Another distance  $d$  bad region is reached.**

In this case, we reach some distance  $d$  bad region  $D_i$  with  $i < m$ . See Figure 10 for an indication. Denote by  $D_{i,1}$  and  $D_{i,2}$  the two parts of  $D_i$  separated by our finger. Then  $D_{i,1}$  is good while  $D_{i,2}$  is a bad region of distance  $d$ . We have  $b(D_{i,2}) = b(D_i) + 1$  and  $b(D_{m,1}) = b(D_m) - 1$ . So the total badness of distance  $d$  remains the same. But we are decreasing the distance  $d$  complexity since we are moving the badness from a later bad region to an earlier bad region. So for the new Heegaard diagram  $\mathcal{H}'$ , we have  $d(\mathcal{H}') = d(\mathcal{H})$  and  $c_d(\mathcal{H}') < c_d(\mathcal{H})$ .

**Case 4. Coming back to  $D_m$ .** This is the worst case and we need to pay more attention. We divide this case into two subcases, according to which edge the finger is coming back through.

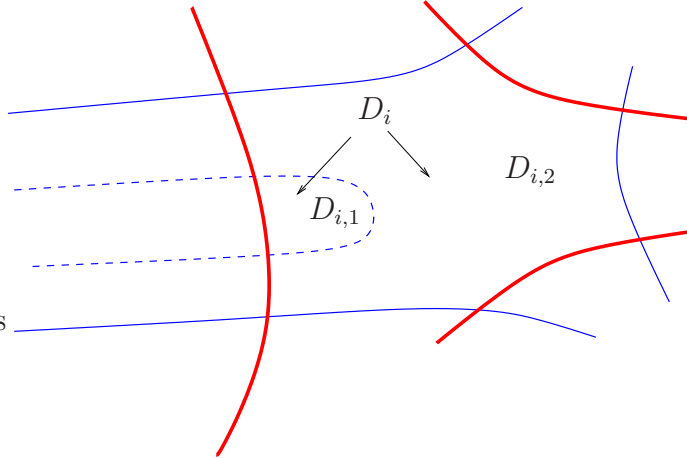


FIGURE 10. **Case 3. Another distance  $d$  bad region is reached.**

**Subcase 4.1. Coming back via an adjacent edge.**

This subcase is indicated in Figure 11. Without loss of generality, we assume the finger comes

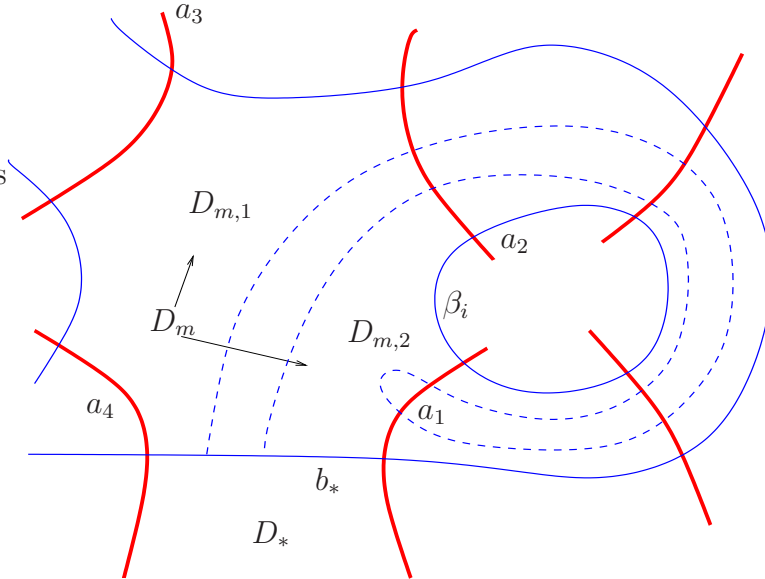


FIGURE 11. **Case 4.1 Coming back via an adjacent edge - finger move.**  
The finger is denoted by the dotted arc.

back via  $a_1$ . In this case, we see the full copy of some  $\beta$  curve, say  $\beta_i$ , one the right side along our long finger. Suppose  $b_* \subset \beta_j$ . Note that  $i \neq j$  since otherwise  $b_* \subset \beta_i$  and we will reach either  $D_m$  or  $D_*$  at an earlier time. Now instead of doing the finger move, we handleslide  $\beta_j$  over  $\beta_i$ . This is indicated in Figure 12.

Note that after the handle slides, we are not increasing the distance of any bad region. We have increased the badness of  $D_*$ , but it is a distance  $d - 1$  region.  $D_{m,2}$  is a bigon region and  $b(D_{m,1}) = b(D_m) - 1$ . So for the new Heegaard diagram  $\mathcal{H}'$  after the handleslide, the total badness of distance  $d$  is decreased by 1. We have  $d(\mathcal{H}') \leq d(\mathcal{H})$  and  $c_d(\mathcal{H}') < c_d(\mathcal{H})$ .

**Subcase 4.2. Coming back via a non-adjacent edge.**

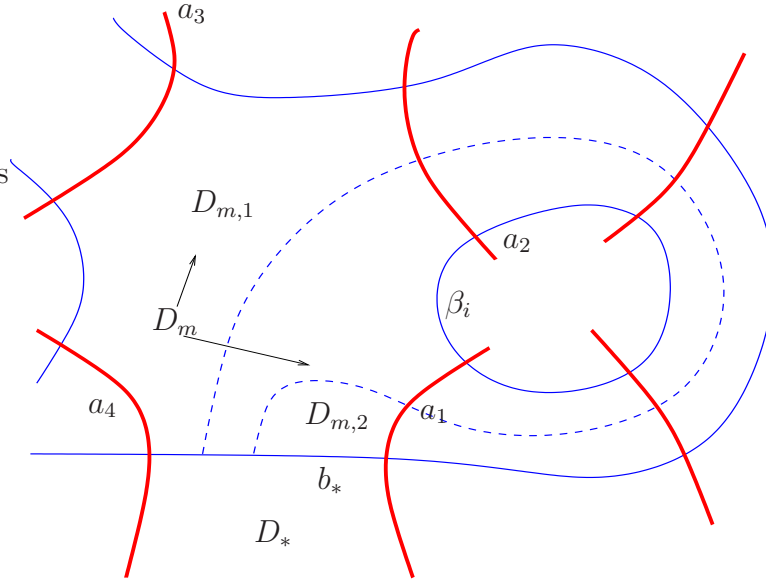


FIGURE 12. **Case 4.1 & 4.2 Coming back via an adjacent edge - handleslide.** The dotted arc denotes the  $\beta$  curve after the handleslide.

If we return through  $a_k$  with  $3 < k \leq n$ , then, instead of the finger move through  $a_2$ , we do a finger move through  $a_3$  (starting from  $b_*$ ). If we reach one of the first three cases, we are decreasing the distance  $d$  complexity by similar arguments as before.

Suppose instead that we are coming back, say via  $a_i$ . We claim that  $3 < i < k$ . Certainly we can not come back via  $a_3$ . The finger can not come back via  $a_k$  since the chain of squares from  $a_k$  is connected to  $a_2$ . If  $i > k$  or  $i < 3$ , we could close the cores the two fingers to get two simple closed curves  $c_1$  and  $c_2$ , as indicated in Figure 13. Then  $c_1$  and  $c_2$  intersect transversely at exactly

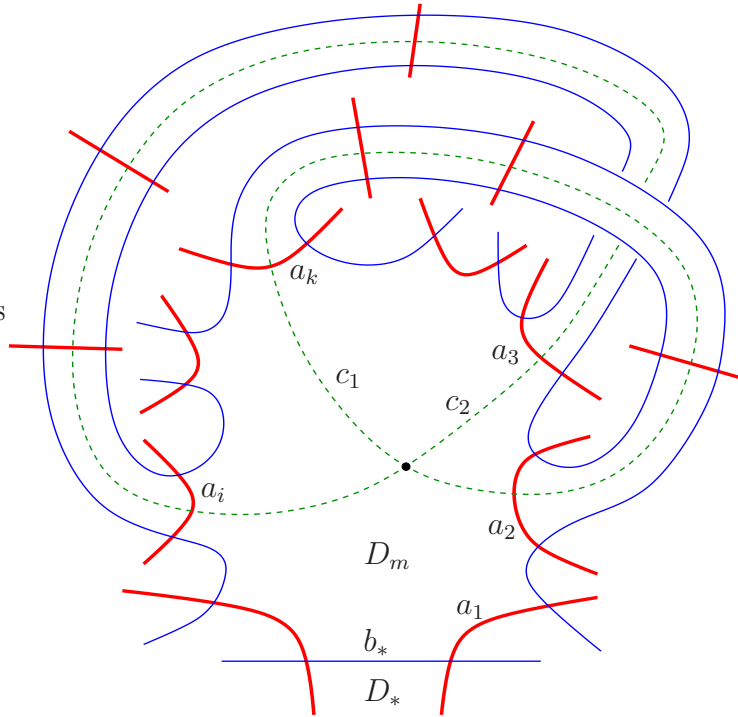


FIGURE 13. **Case 4.2 There are no crossing fingers.** The fingers are not showed here. Instead, the two dotted arcs denote the cores of the two fingers.

one point and they are in the complement of the  $\beta$  curves. The complement of the  $\beta$  curves is a punctured sphere. Attach disks to get a sphere. Then as homology classes, we get  $[c_1] \cdot [c_2] = 1$ . But  $H_1(S^2) \cong 0$ . This is a contradiction. So we must have  $3 < i < k$ . (The argument of this claim was suggested by Dylan Thurston.)

Now, instead of the finger move through  $a_3$ , we do another finger move through  $a_4$ . And continue the same arguments. We either end up with a finger which does not come back, or we get some finger that starts at  $a_j$  and coming back via  $a_{j+1}$ . For a finger not coming back, we reduce to previous cases and the lemma follows.

For a finger starting at  $a_j$  and coming back at  $a_{j+1}$ , we see a full  $\beta$  circle. We do a handleslide as in Subcase 4.1. We have  $b(D_{m,1}) = \max\{n - j - 1, 0\}$  and  $b(D_{m,2}) = \max\{j - 2, 0\}$ . And  $b(D_{m,1}) + b(D_{m,2}) \leq n - 2$ . So for the new Heegaard diagram  $\mathcal{H}'$  after the handleslide, the total badness of distance  $d$  decreases. We have  $d(\mathcal{H}') \leq d(\mathcal{H})$  and  $c_d(\mathcal{H}') < c_d(\mathcal{H})$ .

And we end the proof of our lemma. □

Repeat this process to make  $c_d = (0)$ . And further repeating this process will eventually kill all bad regions other than  $D_0$ .

**4.3. Admissibility.** In this subsection, we show that our algorithm will not change the admissibility, that is, if we start with an admissible Heegaard diagram, then our algorithm ends with an admissible Heegaard diagram. There are two operations involved in our algorithm: isotopies and handleslides, and we will consider them one by one.

The isotopy is the operation in Figure 14. Let  $\mathcal{H}$  and  $\mathcal{H}'$  be the Heegaard diagrams before and

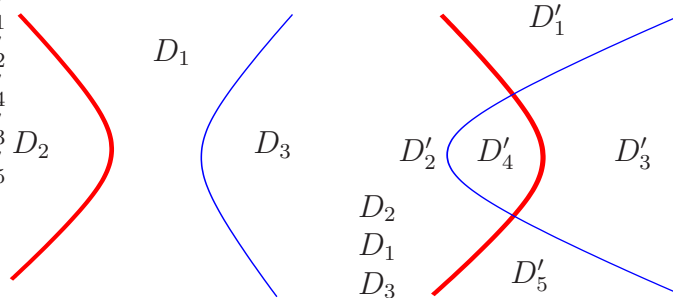


FIGURE 14. **Isotopy of the  $\beta$  curve.**

after the isotopy. Suppose  $\mathcal{H}$  is admissible. For a periodic domain in  $\mathcal{H}'$

$$\phi' = c_1 D'_1 + c_2 D'_2 + c_3 D'_3 + c_4 D'_4 + c_5 D'_5 + \cdots$$

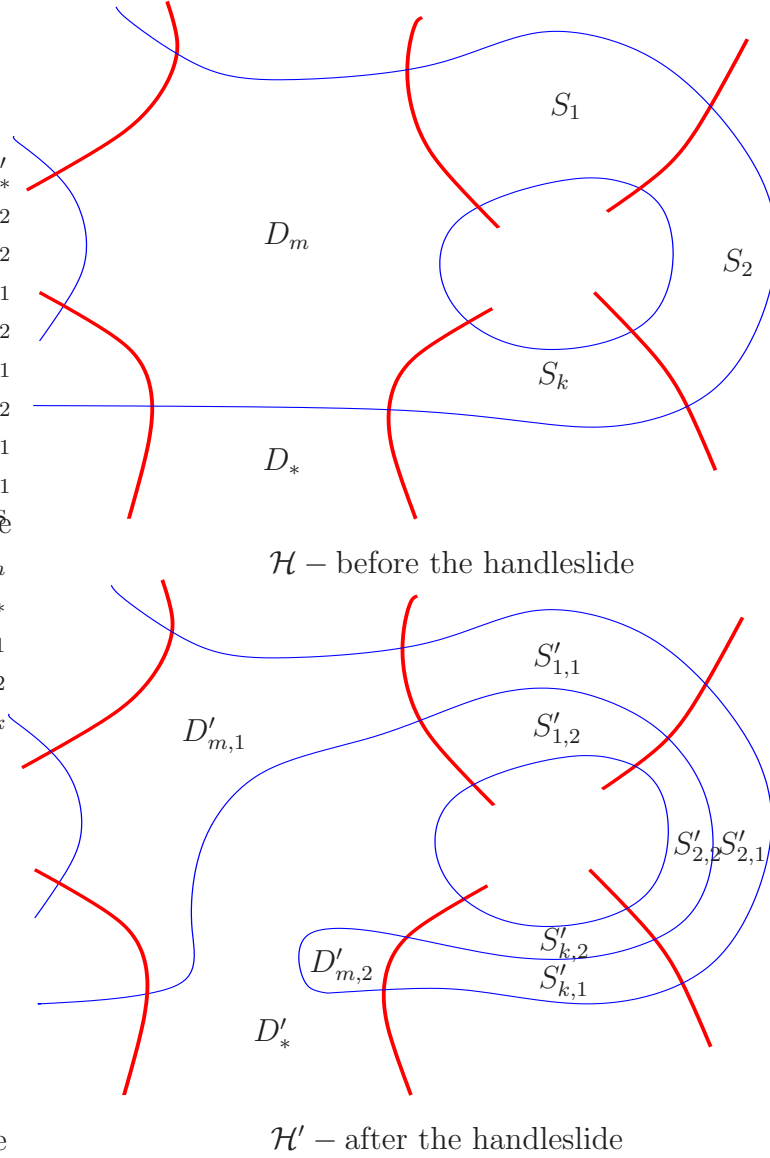
we have  $c_2 - c_1 = c_4 - c_3 = c_2 - c_5$  and  $c_1 - c_3 = c_2 - c_4 = c_5 - c_3$ . Hence  $c_1 = c_5$  and  $c_4 = c_2 + c_3 - c_1$ . Note that the regions are all the same except those in Figure 14. So

$$\phi = c_1 D_1 + c_2 D_2 + c_3 D_3 + \cdots$$

is a periodic domain for  $\mathcal{H}$ . Since  $\mathcal{H}$  is admissible,  $\phi$  has both positive and negative coefficients, and so does  $\phi'$ . Hence  $\mathcal{H}'$  is admissible.

Our handleslide operation is indicated in Figure 15. Let us make notations of the regions as indicated in Figure 15. Suppose  $\mathcal{H}$  is admissible. For a periodic domain in  $\mathcal{H}'$

$$\phi' = c_* D'_* + c_1 D'_{m,1} + c_2 D'_{m,2} + c_{1,1} S'_{1,1} + c_{1,2} S'_{1,2} + \cdots + c_{k,1} S'_{k,1} + c_{k,2} S'_{k,2} + \cdots$$

FIGURE 15. **Handleslide of the  $\beta$  curve.**

We will get  $c_1 - c_* = c_{1,1} - c_{1,2} = \cdots = c_{k,1} - c_{k,2} = c_2 - c_*$ . Suppose  $c_1 - c_* = c_0$ , then  $c_{i,1} = c_{i,2} + c_0$  and  $c_1 = c_2$ . Now

$$\phi = c_* D_* + c_1 D_m + c_{1,1} S_1 + \cdots + c_{k,1} S_k + \cdots$$

is a periodic domain for  $\mathcal{H}$ . Since  $\mathcal{H}$  is admissible, we get that  $\phi$ , and hence  $\phi'$ , has both positive and negative coefficients. So  $\mathcal{H}'$  is admissible.

**Remark.** In fact, it is showed that nice Heegaard diagrams are always (weakly) admissible ([4, Corollary 3.2]).

**4.4. Summary.** Starting with an admissible one-pointed Heegaard diagram, our algorithm described in Section 4.2 gives an admissible Heegaard diagram with only one bad region, a  $2n$ -gon containing the basepoint  $w$ .

We have similar conclusions for Heegaard diagrams with multiple basepoints. Our algorithm could be modified to get nice admissible Heegaard diagrams. Note that every region is connected

to exactly one region containing some  $w$  point in the complement of the  $\alpha$  curves, so we can define the distance and hence the complexity in the same way, and thus our algorithm works as before.

Thus we proved Theorem 1.2.

5. EXAMPLES

In this section, we give two examples to demonstrate our algorithm. One is on knot Floer homology and the other is on the Heegaard Floer homology of three-manifolds.

5.1. **The Trefoil.** We start with the Heegaard diagram in Figure 16, where the two circles labeled by  $\alpha$  are identified to get a genus one Heegaard diagram.

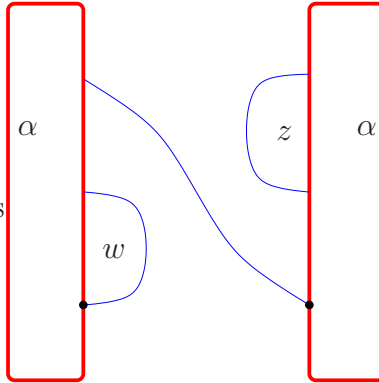


FIGURE 16. **A Heegaard diagram for the trefoil knot.** We make the convention that every two thicker circles with the same  $\alpha$  labels are identified so that the two dark points on them are identified.

After isotopy using the algorithm in Section 4, we end up with the Heegaard diagram as in Figure 17. So we have nine generators. It is routine to find all boundary holomorphic disks and determine

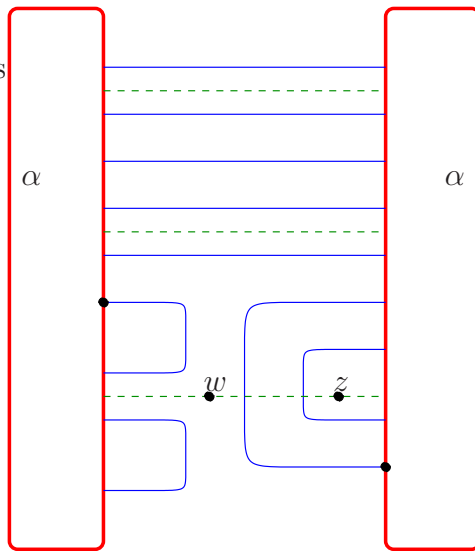


FIGURE 17. **A nice Heegaard diagram for the trefoil knot.** We use the same convention as in Figure 16. The trefoil is given by the dotted curve.

the Alexander and Maslov gradings of each generator.

5.2. **The Poincaré homology sphere  $\Sigma(2, 3, 5)$ .** We start with the Heegaard diagram of  $\Sigma(2, 3, 5)$  in Figure 18, viewed as the +1 surgery on the right-handed trefoil knot. By cutting the Heegaard

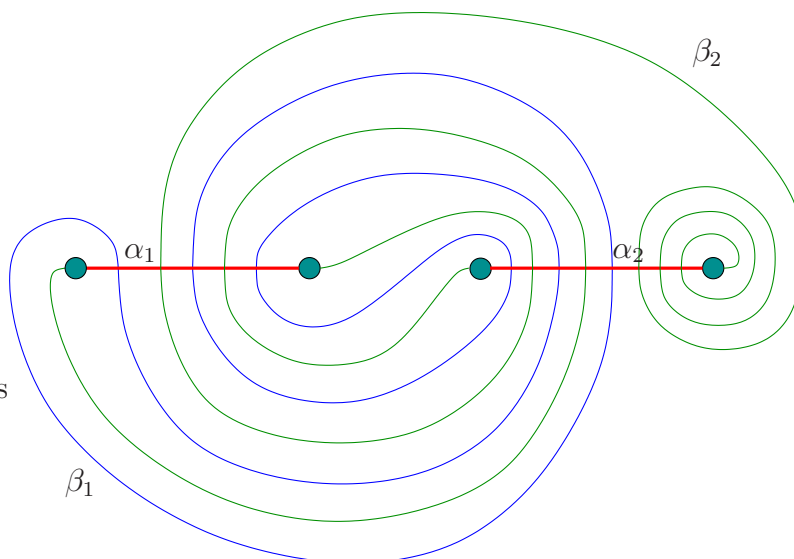


FIGURE 18. **A Heegaard diagram for the Poincaré homology sphere.** The left two darkly shaded circles are the feet of one handle, and the right two darkly shaded circles are the feet of the other handle.

surface along the  $\alpha$  circles, we get a planar presentation of the Heegaard diagram in Figure 19. It is

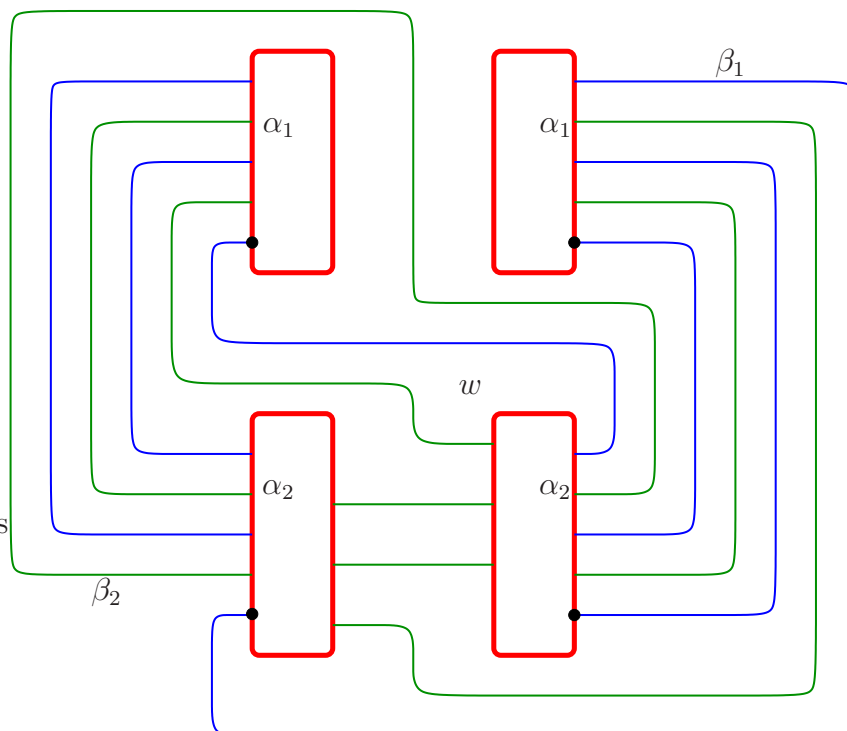


FIGURE 19. **A Heegaard diagram for the Poincaré homology sphere.** We use the same convention as in Figure 16.

easy to see that there are 21 generators for the chain complex. However, the authors do not know how many differentials there are for it.

After applying our algorithm, we get a nice Heegaard diagram as in Figure 20. There are 335 generators and 505 differentials for this diagram. We leave the actual computation using this diagram to the patient reader.

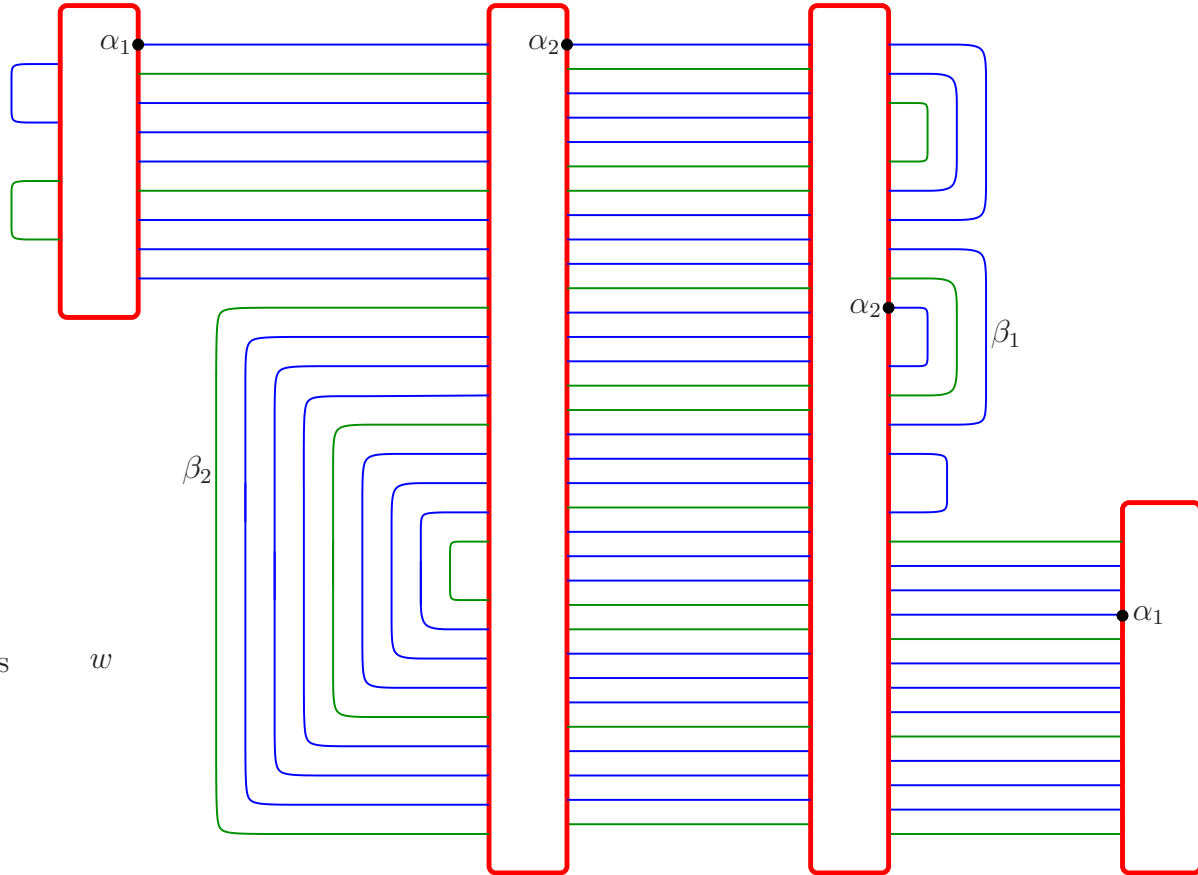


FIGURE 20. A nice Heegaard diagram for the Poincaré homology sphere. We use the same convention as in Figure 16.

#### REFERENCES

- [1] Paolo Ghiggini. Knot Floer homology detects genus-one fibred knots. To appear in *American Journal of Mathematics*, arXiv:math.GT/0603445, 2006.
- [2] András Juhász. Floer homology and surface decompositions. arXiv:math.GT/0609779, 2006.
- [3] Robert Lipshitz. A Cylindrical Reformulation of Heegaard Floer Homology. *Geometry and Topology*, 10:955–1097, 2006.
- [4] Robert Lipshitz, Ciprian Manolescu, and Jiajun Wang. Combinatorial cobordism maps in hat Heegaard Floer theory. arXiv:math.GT/0611927, 2006.
- [5] Ciprian Manolescu, Peter S Ozsváth, and Sucharit Sarkar. A combinatorial description of knot Floer homology. arXiv:math.GT/0607691, 2006.
- [6] Yi Ni. Knot Floer homology detects fibred knots. arXiv:math.GT/0607156, 2006.
- [7] Peter S Ozsváth and Zoltán Szabó. Holomorphic disks and topological invariants for closed three-manifolds. *Annals of Mathematics (2)*, 159(3):1027–1158, 2004.
- [8] Peter S Ozsváth and Zoltán Szabó. Holomorphic disks and three-manifold invariants: properties and applications. *Annals of Mathematics (2)*, 159(3):1159–1245, 2004.

- [9] Peter S Ozsváth and Zoltán Szabó. Absolutely graded Floer homologies and intersection forms for four-manifolds with boundary. *Advances in Mathematics*, 173(2):179–261, 2003.
- [10] Peter S Ozsváth and Zoltán Szabó. Holomorphic triangles and invariants for smooth four-manifolds. *Advances in Mathematics*, 202(2):326–400, 2006.
- [11] Peter S Ozsváth and Zoltán Szabó. Holomorphic disks and knot invariants. *Advances in Mathematics*, 186(1):58–116, 2004.
- [12] Peter S Ozsváth and Zoltán Szabó. Holomorphic disks and genus bounds. *Geometry and Topology*, 8:311–334, 2004.
- [13] Peter S Ozsváth and Zoltán Szabó. Knot Floer homology and the four-ball genus. *Geometry and Topology*, 7:615–639, 2003.
- [14] Peter S Ozsváth and Zoltán Szabó. Holomorphic disks, link invariants and the multi-variable Alexander polynomial. arXiv:math.GT/0512286, 2005.
- [15] Peter S Ozsváth and Zoltán Szabó. Link Floer homology and the Thurston norm. arXiv:math.GT/0601618, 2006.
- [16] Peter S Ozsváth and Zoltán Szabó. Heegaard diagrams and Floer homology. To appear in *the Proceedings for ICM-2006 Madrid*, arXiv:math.GT/0602232, 2006.
- [17] Jacob Rasmussen. Floer homology and knot complements. Ph.D Thesis, Harvard University, 2003.

DEPARTMENT OF MATHEMATICS, PRINCETON UNIVERSITY, PRINCETON, NJ 08544  
*E-mail address:* `sucharit@math.princeton.edu`

DEPARTMENT OF MATHEMATICS, UNIVERSITY OF CALIFORNIA AT BERKELEY, BERKELEY, CA 94720  
*E-mail address:* `wang@math.berkeley.edu`